Chemical Engineering Journal 499 (2024) 156135

Contents lists available at ScienceDirect

Chemical Engineering Journal

journal homepage: www.elsevier.com/locate/cej

Single-step preparation of activated carbons from pine wood, olive stones and nutshells by KOH and microwaves: Influence of ultra-microporous for high CO_2 capture

Gabriela Duran-Jimenez [a,*], Jose Rodriguez [a], Lee Stevens [a], Sanad Altarawneh [a], Andrew Batchelor [a], Long Jiang [b], Chris Dodds [a]

[a] Faculty of Engineering, the University of Nottingham, University Park, Nottingham, NG7 2RD, UK
[b] School of Pharmacy, University of Nottingham, University Park Nottingham, Nottingham NG7 2RD, UK

ARTICLE INFO

Keywords:
CO_2 capture, microwaves
Activated carbon
Olive stones
Pine wood
Pecan nutshells
Ultra micropores

ABSTRACT

Biomass residues are crucial feedstocks for facing climate change challenges due to high-value products, such as producing activated carbons (AC) for carbon capture. Two stages of pyrolysis followed by activation at high temperatures are the most used technique for converting lignocellulosic precursors into porous activated carbons. This process has shown to offer the highest surface areas; however, a two-stage process is undesirable as is an energy-intensive processes. Product characteristics are affected by feedstock and reaction rate conditions. In the present study pine wood (PW), olive stones (OS) and pecan nutshells (NS) were evaluated as feedstocks in the production of AC for selective post-combustion CO_2 capture via a single-step pyrolysis-activation using microwave heating. Direct raw biomass impregnation was completed using potassium hydroxide (KOH). The ACs were synthesised in 8 min using 300 W of microwave power with 8.8 GJ t^{-1} specific microwave energy input. Samples exhibited large specific surface areas (S_{BET}), up to 1340 m^2g^{-1}, with 70 % of ultra-micropores (<0.8 nm), fundamental for high CO_2 adsorption capacity. Among the tested biomasses, PW was the best performing and physicochemical characterisation and CO_2 capture studies indicated that PW-based AC has 79 % carbon, amorphous structure, and possessed larger ultra-micropores that resulted in high CO_2/N_2 selectivity (12.5), and one of the largest CO_2 uptakes for ACs (6.2 and 4.2 mmol/g at 0 and 25 °C, respectively). The CO_2 performance was investigated across a range of temperatures up to 100 °C, while cyclic regenerative performance was confirmed after 15 adsorption–desorption cycles. This study highlights the development of AC from different lignocellulosic resources by a fast and low-energy single microwave-pyrolysis activation process that can produce ultra-microporous structures implemented in post-combustion CO_2 capture.

1. Introduction

The increasing concentration of carbon dioxide in the atmosphere is the main contributor to global warming, which, combined with the growing global energy demand, poses a significant challenge for climate change mitigation [1,2]. Governments worldwide have committed to net-zero emissions by 2050 [3], and large-scale carbon capture technologies are pivotal in transitioning to sustainable development. Solid adsorption using carbon materials is a promising technology for post-combustion CO_2 capture due to its high CO_2 uptake capacity, selectivity, and economic regeneration [4,5].

Activated carbons (ACs) are among the most used materials in industrial applications due to their remarkable properties, including large surface area, surface chemistry, recyclability, thermal and chemical stability, mechanical robustness, and tuneable properties. More recently, the usage of ACs for carbon capture has gained traction due to their techno-economic prospects [6–8]. Due to the depletion and environmental consequences associated with using coal and lignin as conventional feedstocks for producing ACs, lignocellulosic biomass has emerged as a sustainable alternative, contributing to waste management and valorisation [9–12].

Traditionally, the preparation of AC from biomass involves two steps: First, a biochar is prepared at a low heating rate (>10 °C min^{-1}) and low temperatures (400–600 °C) [13,14]. The produced biochar is

* Corresponding author.
E-mail address: gabriela.duranjimenez1@nottingham.ac.uk (G. Duran-Jimenez).

https://doi.org/10.1016/j.cej.2024.156135
Received 22 August 2024; Received in revised form 22 September 2024; Accepted 23 September 2024
Available online 24 September 2024

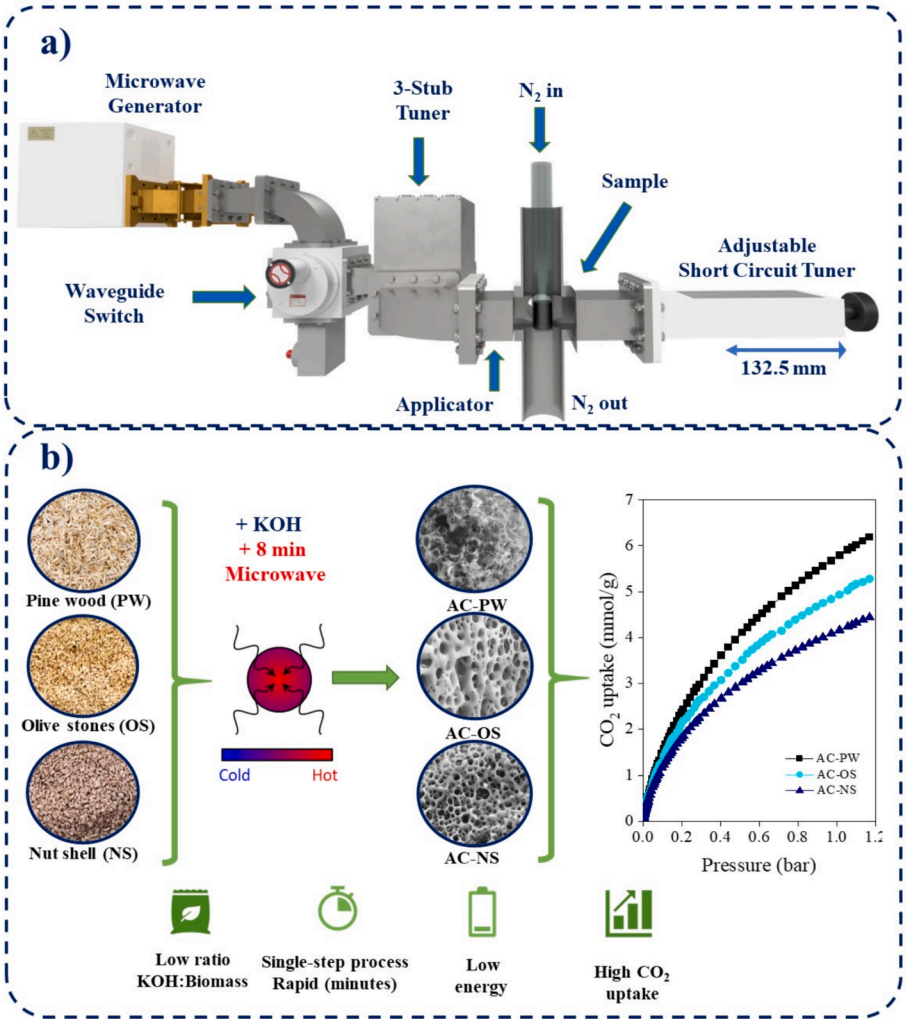

Fig. 1. Schematic of the microwave setup (a) and single-step method utilised for the preparation of the AC samples (b).

then activated at high temperatures (700–900 °C) using physical or chemical activators to develop internal porosity and large specific surface areas. Physical activation commonly occurs at temperatures of more than 800 °C using gas oxidants such as steam or CO_2 to unlock pores and create a large surface area. In chemical activation processes, the biochar is impregnated with a chemical activation agent that helps form defined porous structures. These pathways involve relatively long processing times, typically ranging from 3-10 h resulting in high energy consumption [12,15–17]. Recently, a simple method has attracted attention, where the AC can be prepared in one-step. In this method, the mixture of biomass with an activator is subjected to a slow heating rate at high pyrolysis temperatures (700–900 °C). Findings suggest the one-step can reduce pyrolytic oil production [18] and significantly reduce the operating costs involved in multi-step preparation [19]. Although certain studies have reported direct biomass impregnation to produce ACs, these studies still involve long processing times (3–5 h) in conventional heating and have focused on the catalytic effect of potassium hydroxide (KOH) and biomass.

In our previous studies, an alternative using a single-step process for pyrolysis and activation using microwave heating as a heating source has been developed [4,5], which greatly reduces processing time to <8 min and energy consumption whilst achieving similar or even better product quality, compared with long and multi-step conventional synthesis [14].

Microwaves deliver heat directly within the material volume, resulting in fast volumetric heating, contrary to conventional heating sources, which deliver heat to the material's surface relying on thermal conduction to propagate the energy through it. In the case of biomasses, heat conduction is typically slow due to biomass's low thermal conductivity, which results in limited bed size and reduced plant throughput. These limits are a function of the material's dielectric properties and frequency, and their determination is fundamental [20–22]. Previous studies report the addition of susceptors or microwave absorber such as carbon, graphite and silicon carbide to increase microwave interaction with biomass and to enhance product formation [23]. To the best of the authors' knowledge, the role of direct biomass impregnation, removing the need for pre-carbonisation and removing the use of susceptors in biomass wastes for AC formation using microwave heating is not available in the literature as intended in this work. In our previous study, the systematic evaluation of microwave processing conditions evidenced that it is possible to produce AC with large microporosity from (1:1 mass ratio) KOH impregnated pecan nutshell (NS), in a simple, rapid and sustainable manner [5]. This work aims to develop a further understanding of the interaction between a range of impregnated biomass such as pine wood (PW), olive stones (OS), and pecan nutshells (NS) and microwaves, and the evaluation of the single-step microwave pyrolysis-activation process to produce ACs for carbon capture. These biomasses have been selected due to their abundance and sustainable source nature within the concept of circular economy [24,25]. Among the available activators, KOH is very promising due to its capacity to develop highly microporous structures and high carbon yields [18]. The pore development is the result of redox reactions where

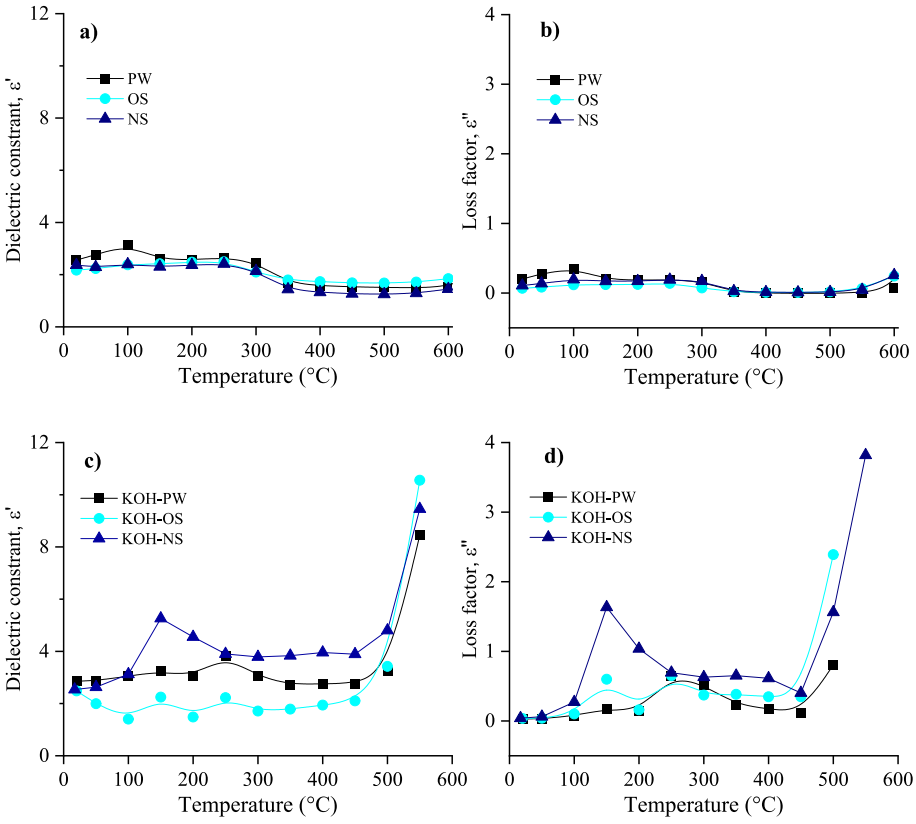

Fig. 2. Dielectric constant and loss factor of feedstock biomass (a) and (b) and impregnated biomass (c) and (d).

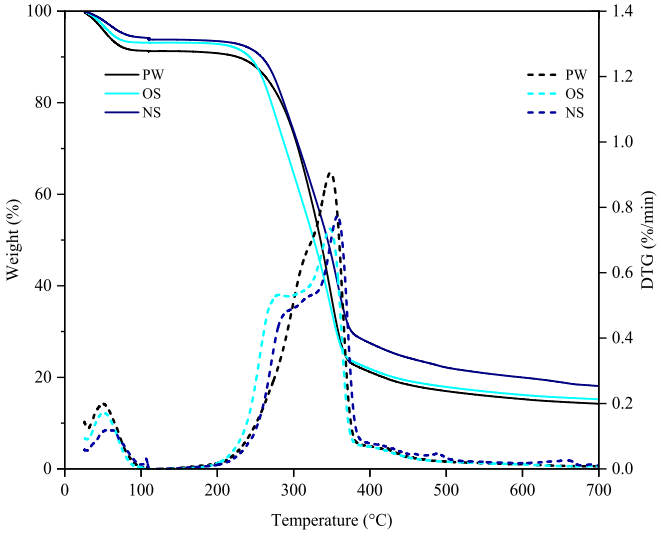

Fig. 3. TGA and derivative thermogravimetry (DTG) of pine wood (PW), olive stones (OS) and pecan nutshells (NS).

Table 1
Proximate analysis of biomass used in the preparation of AC in this study.

Sample	Pine wood (PW)	Olive stones (OS)	Pecan nutshell (NS)
Moisture (%)	8.74	6.90	6.20
Volatile Matter (%)	79.57	83.09	77.20
Fixed Carbon (%)	10.93	9.92	14.78
Ash (%)	0.76	0.09	1.82

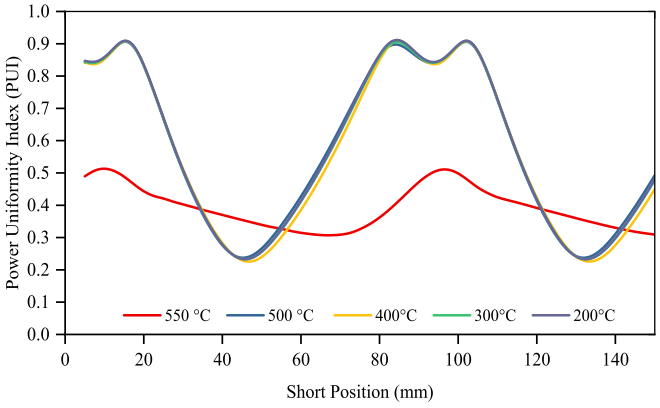

Fig. 4. PUI for sliding short lengths and sample properties for 200, 400, 500, and 550 °C.

the gaseous products such as CO_2, H_2 and CO react with carbon, while the hydroxide itself gets reduced to metallic potassium intercalating into the carbon frameworks and expanding the carbon lattices [5,26].

This work presents for first the time, a rapid synthesis of ultra-microporous ACs in only 8 min for different biomasses, using a relatively low KOH impregnation ratio (2:1) in comparison with literature (4:1, 5:1) [27]. In this study, dielectric properties and electromagnetic simulations were conducted to optimise the microwave experimental setup. The feasibility of ACs for post-combustion CO_2 capture was evaluated, providing insights on the effects of physico-chemical properties from different biomass feedstocks to attain high CO_2 uptake, fast kinetics of adsorption, selectivity and reusability after cyclic adsorption–desorption experiments.

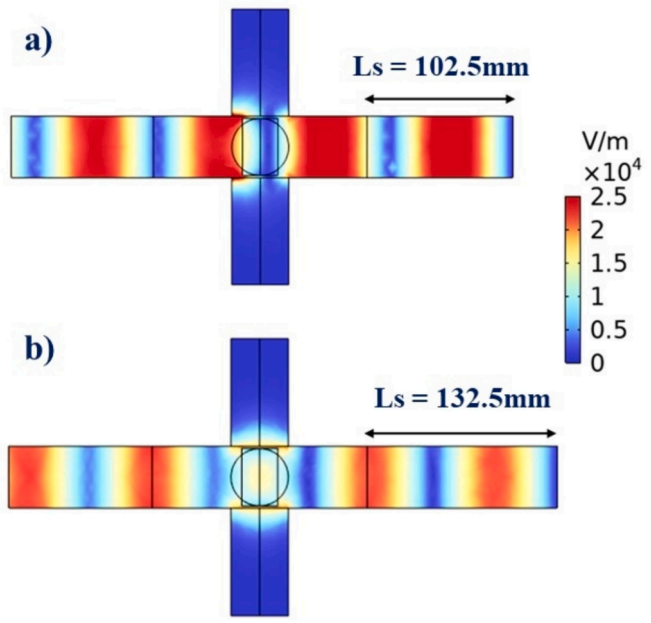

Fig. 5. Electric field distribution for sliding short of length (a) 102.5 mm and (b) 132.5 mm for sample properties at 500 °C.

Table 2
AC yields and specific microwave energy input required for their preparation.

Sample name	*Energy (GJ t^{-1})	*AC yield (%)
AC-PW	8.8 ± 0.05	63.8 ± 0.2
AC-OS	8.6 ± 0.1	67.2 ± 0.4
AC-NS	9.0 ± 0.2	62.1 ± 3.8

* Standard error between replications. The AC yield was calculated based on weight% of activated carbon related to the weight of raw material.

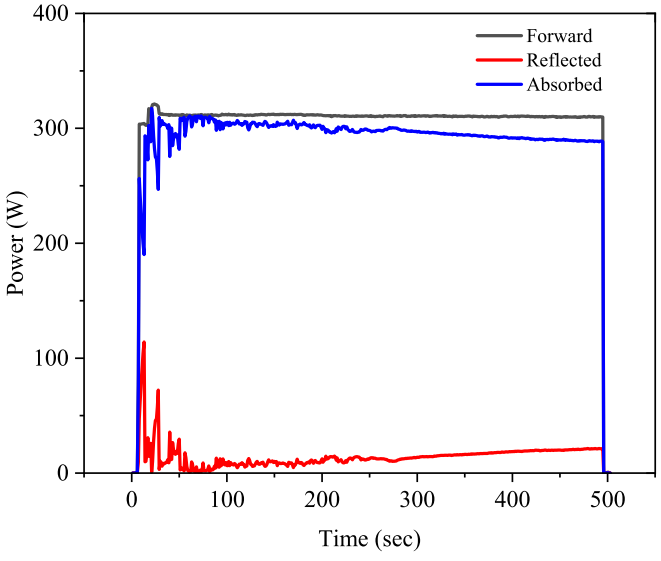

Fig. 6. Forward, reflected and absorbed power during microwave synthesis of AC-NS sample.

2. Experimental

2.1. Materials

Three waste-biomasses derived from pine wood (PW), olive stones (OS), and pecan nutshell (NS) were used as AC precursors in this study. The three precursors were milled and sieved to obtain a mean particle size of ~ 0.7 mm, washed with deionised water, and dried in an oven at 80 °C for 24 h. All biomasses were physically mixed with potassium hydroxide pellets of analytical grade (>85 %) using an impregnation ratio of 2:1 (KOH:biomass).

2.2. Preparation of activated carbon using a single-step and microwave heating

Pyrolysis-activation via a single microwave step was carried out in inert atmosphere in a system represented in Fig. 1. A quartz sample tube of 25 mm internal diameter was used as a reactor. The selection of quartz was to ensure to have a microwave transparent reactor able to withstand elevated temperatures. In total, 15 g of impregnated sample (biomass and KOH) was placed on a reactor that contained a sintered gas distributor plate. The quartz tube was then inserted into a rectangular single-mode microwave applicator through a choke tube. This metallic tube was designed to prevent microwave leakage above health and safety limits (50 Wm^{-2}, measured 50 mm from the tube opening) while allowing the sample tube into the cavity and enabling gas evacuation from the process. The design of the applicator was conducted to ensure the system can create high-power densities in the heated phases, excellent treatment uniformity, and stable operation without degenerated modes or polarization rotation as suffered by other commonly used circular resonator cavities [28]. This type of applicator provides a well-defined electric field distribution and higher intensity compared to multi-mode systems such as commercial kitchen microwaves and is best suited for repeatable treatment of relatively small samples [28]. The applicator is connected to a 2 kW, 2.45 GHz microwave generator (Sairem®) by WR430 aluminium waveguides. A 3-stub microwave tuner (S-TEAM) with inbuilt power meters was used to ensure efficient delivery of power to the samples and record incident (P_i) and reflected power (P_r). The tuner was adjusted at the beginning of each experiment.

ACs were prepared under an N_2 atmosphere flowing at 1 L min^{-1}, flushed from the top to avoid fluidising the sample and remove the gases from the reaction zone. ACs were prepared using 300 W for 8 min. These conditions were selected based on our previous findings, where systematic evaluation of microwave power, time, energy and impregnation ratio has been discussed [5,11,14,29]. Once the target time was reached, a K-type thermocouple was used to measure surface temperature in a single point as a reference. The sample was then kept in an inert atmosphere for 5 min to cool down.

The specific microwave energy input (on a biomass basis) was calculated from the numerical integration of the absorbed power (P_a) following Equation (1):

$$E_{MS} = \frac{\int P_a dt}{M} \quad (1)$$

Where E_{MS} is the specific absorbed energy (GJ t^{-1}), t is the time (s), P_a is the absorbed power (kW) being the difference of the incident and reflected power ($P_a = P_i - P_r$), and M is the initial mass of the sample (g).

To calculate the yield, the final carbon was repeatedly washed with deionised water until neutral pH was obtained and then dried at 105 °C overnight. The results presented here are the average of 3 triplications. For convenience, the activated carbons were labelled as "AC-XX", where XX is the abbreviation for the biomass precursor used in the carbon synthesis.

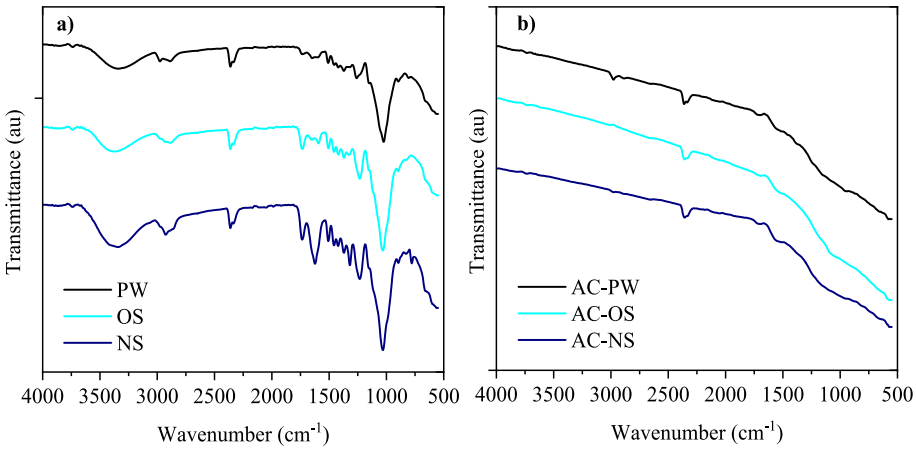

Fig. 7. FT-IR of (a) biomass and (b) AC prepared in this study (pine wood, (PW), olive stones (OS) and pecan nutshell (NS).

2.3. Dielectric properties measurement

The main microwave interaction mechanisms for the type of materials under study are dielectric polarisation, ionic conduction, interfacial polarisation and Joule effects [30–32]. These interactions can be quantified within its effective dielectric properties, which can be represented in the form of a complex relative permittivity as:

$$\varepsilon_r = (\varepsilon_r' - j\varepsilon_r'' \quad (2)$$

The complex relative permittivity comprises a real part called the relative dielectric constant (ε_r'), and an imaginary part known as the relative dielectric loss factor (ε_r''). The former measures the material's ability to store electrical energy, and the latter represents the ability to transform the energy into heat within the material.

Dielectric properties and the temperature dependence of biomasses PW, OS and NS and the KOH-impregnated biomasses (KOH-PW, KOH-OS and KOH-NS) were obtained using the cavity perturbation technique [33] for a temperature range of 20–500 °C at 2450 MHz under nitrogen. This technique was selected due to is suited for granular materials, elevated temperature and close to ISM (Industrial, Scientific and Medical) frequency. The system is composed of a tube furnace and cylindrical TM_{0n0} mode cavity. An automated step motor was used to move the sample rapidly from the furnace to the cavity, where the dielectric properties were measured by an HP 8753 vector network analyser (VNA) at the desired temperature. The sample was placed in a microwave transparent quartz tube of 3 mm (ID), and the dielectric properties were calculated using the difference resonant response of the cavity when loaded and empty. The results presented in this work show an average of three replicate samples for each case.

2.4. Optimisation of experimental setup for microwave activation

To ensure the energy delivered by the microwave system is absorbed into the sample, the optimal sliding short circuit tuner (adjustable short) position was evaluated. This ensures effective coupling and treatment homogeneity in single-mode microwave systems. Numerical optimisation was used to obtain the position based on COMSOL Multiphysics RF module using the finite element method (FEM) [34].

The system was modelled with a maximum element size of $\lambda/5$, and a finer $\lambda/10$ element size within the material, where λ represents the wavelength inside of the material (i.e. $\lambda = \lambda_0/\sqrt{\varepsilon_r'}$, with λ_0 being the free-space wavelength). Given that no suitable available data for these materials was found in the literature, the dielectric properties measured in this work were used and samples were modelled using isotropic media. A parametric sweep of the short position was performed for different material properties within the expected range to determine the position that can provide superior overall uniformity of treatment for most cases. The uniformity is assessed using the power uniformity index (PUI), which measures the uniformity of power dissipation within a volume; zero means an entirely uniform distribution of power dissipation (i.e. zero standard deviation) [28,35].

2.5. Characterisation techniques

2.5.1. Proximate, ultimate and surface functional analysis

To determine the content of volatile matter, fixed carbon, and ash (proximate analysis) in the biomasses employed, thermogravimetric experiments were performed in triplicate using a TA Instruments Q500 thermogravimetric analyser (TGA). An approximate 10 mg sample was heated to 900 °C under a nitrogen atmosphere at a flow rate of 100 mL min^{-1} and 1 bar for 15 min. The atmosphere was then switched to air and held for a further 15 min. The ultimate analysis was conducted in a LECO CHN 628 analyser according to the ASTM D5373-21 protocol, where oxygen was calculated by difference. The chemical functionalities of the feedstocks and ACs were identified using Fourier-Transform Infrared (FTIR) spectroscopy (ThermoScientific Nicolet iS10) with attenuated total reflectance (ATR) accessory. The FTIR spectra were recorded from 4000 to 400 cm^{-1} with a resolution of 4 cm^{-1}. X-ray photoelectron (XPS) measurements were performed using a Kratos Liquid Phase Photoelectron Spectroscopy (LiPPS) with a monochromated Al kα X-ray source (1486.6 eV) operated at 10 mA emission current and 12 kV anode potential (120 W). Pass energy was 160 eV for wide scans and 20 eV for high resolution scans. Wide scans were run with a step size of 0.5 eV and high-resolution scans were run with a step size of 0.1 eV. Data processing was carried out using CASAXPS software (version 2.3.24) with Kratos sensitivity factors (RSFs) to determine atomic % values from the peak areas.

2.5.2. Textural, morphological and crystallographic characterisation

The textural properties of the ACs were obtained from the adsorption isotherms of N_2 at −196 °C using a Micromeritics ASAP 2420 apparatus from 0.00005 to 0.99 relative pressure (P/P_0). Approximately 250 mg of samples were weighed into a sample tube and degassed for 15 h at 120 °C. The surface area was calculated using the Brunauer–Emmett–Teller (BET) theory, based on adsorption data in the range of 0.01–0.1P/P_0 following previous reported methodology [14]. The ultra-micropore (<0.8 nm), micropore (<2 nm) and total pore volumes and size distributions were determined by Non-Local Density Functional Theory (NLDFT) on carbon slit pores by combining a CO_2 adsorption isotherm at 0 °C to a N_2 adsorption isotherm beginning at 0.0005P/P_0 using Microactive Software V5.0.

X-ray diffraction (XRD) analysis was performed on a Bruker D8 Advance Da Vinci diffractometer, with 0.02° step size and step time of

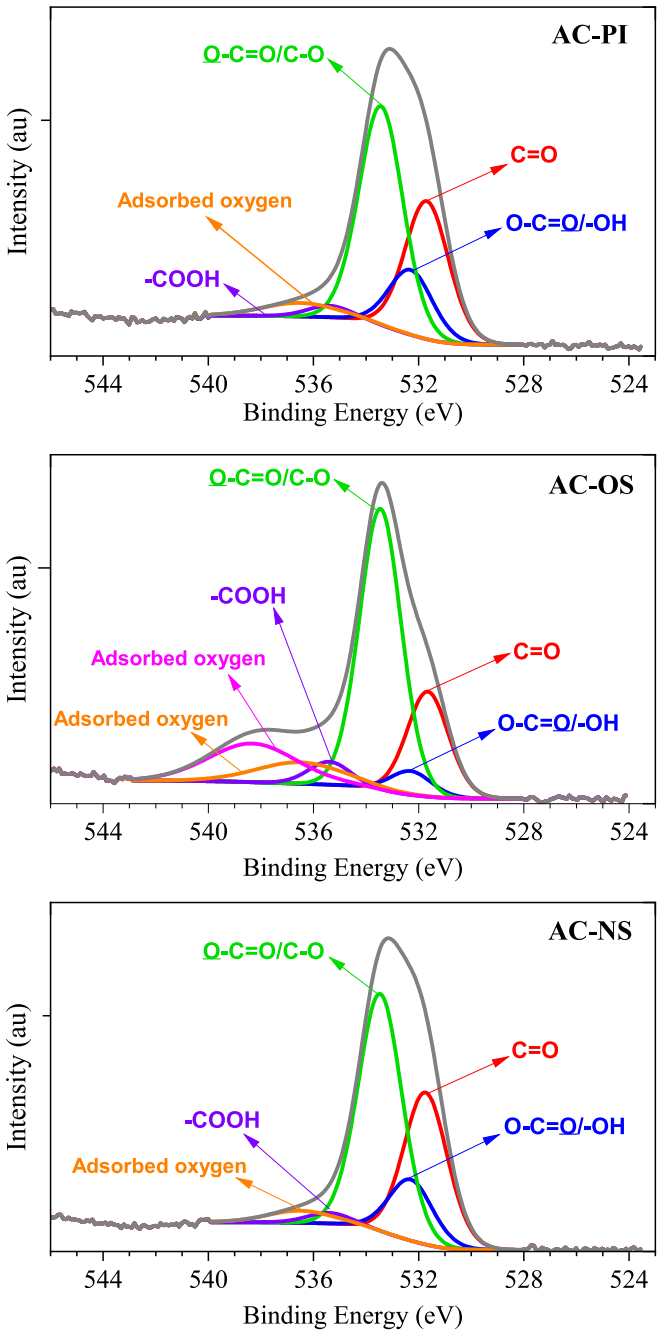

Fig. 8. X-ray photoelectron spectroscopy (XPS) and O-containing species (O 1s spectra) of activated carbons.

10 sec in the 2θ range 10−80°. The morphology of the samples was examined by Scanning Electron Microscopy (SEM) using a Philips XL 30 microscope.

The fraction of micropore filling by CO_2 (f_{CO2}) is a parameter that describes the relationship between the pore size and the pore filled by CO_2, and was calculated as [5]:

$$f_{CO2} = q(V_{<2nm} \cdot \rho_{CO2}) \quad (3)$$

where q is the CO_2 uptake, $V_{<2nm}$ is the micropore volume and ρ_{CO2} is the density of liquid CO_2 (1.03 g cm^{-3} at 0 °C).

2.6. Post-combustion CO_2 capture experiments

The CO_2 capture studies were performed using volumetric and gravimetric methods. Isotherms were obtained at 0 and 25 °C on a volumetric Micromeritics ASAP 2420 analyser. In this case, the samples were previously degassed at 120 °C for 15 h and the adsorption capacity was investigated in terms of the adsorbed amount (CO_2 100 %) per gram in the pressure range of 0.001–1.2 bar.

The thermogravimetric CO_2 uptake was carried out using a TA Instruments Q500 TGA. The carbon samples were dried at 120 °C under nitrogen at 100 ml min^{-1} for 30 min before being cooled to the set adsorption temperature. The CO_2 uptake was evaluated at a variety of temperatures between 25 and 100 °C, in 100 % CO_2. Once the adsorption reached equilibrium at a given temperature, the sample was heated to 120 °C for 15 min to complete the CO_2 desorption. Cyclic adsorption and desorption tests were also conducted to determine the stability and reusability of the AC produced.

To determine the selectivity of ACs thermogravimetric analysis were conducted using N_2 and CO_2. Both set of experiments were conducted at 25 °C and the sample was dried under argon at 120 °C and the gas was switched from argon to nitrogen. The isosteric heat of adsorption (Q_{st}) was calculated using CO_2 adsorption isotherms measured at 0 and 25 °C based on the Clausius-Clapeyron equation:

$$ln\left(\frac{P_2}{P_1}\right) = \frac{Q_{st}}{R}\left(\frac{1}{T_1} - \frac{1}{T_2}\right) \quad (4)$$

where Pi is pressure for isotherm i; T_i is temperature for isotherm i; R is the universal gas constant 8.315 J $K^{-1}mol^{-1}$ [5].

3. Results and discussion

3.1. Dielectric and thermal properties

The applicability of microwave heating technologies depends partially on the dielectric properties of the materials to be processed. The measured dielectric properties of the raw biomass and impregnated biomass samples with temperature are shown in Fig. 2. All the tested biomass samples exhibit similar behaviour of relatively low and stable dielectric constant and loss up to 550 °C. Above 550 °C, dielectric properties increase rapidly due to the carbonisation of the biomass into char. Chars are a highly microwave absorbent attributable to high π-electrons mobility on the carbon structure, increasing its electrical conductivity [36]. It is evident that the impregnated samples have higher dielectric constant and loss factor compared with raw biomass. The increase of dielectric properties seemingly starts at a lower temperature of 450 °C, which can be attributed to the temperature at which KOH converts into K_2CO_3 in the activation process [37].

The main changes in dielectric properties can be associated with the thermal transformation of lignocellulosic biomass, as depicted in Fig. 3 and Table 1. It can be observed that thermograms display mass losses corresponding to moisture, cellulose, and hemicellulose polymers. Proximate analysis shows that NS biomass has a higher content of ash, and this is associated with rich calcium oxalate in biomass [36].

3.2. Comsol multiphysics simulations

3.2.1. Short circuit position determination

Challenges exist to implementing high-temperature microwave processes with changing dielectric properties to achieve uniform processing. For this reason, it is fundamental to understand the sample under treatment conditions and its behaviour within the microwave heating system. In this work, a sliding short circuit tuner (adjustable short) was used to adjust the electromagnetic fields within the applicator to optimise the sample treatment. The uniformity was assessed using the power uniformity index (PUI) considering the dielectric properties shown in Fig. 2, and considering isothermal for 200, 300, 400, 500, and 550 °C. The sample holder made of quartz was modelled considering a permittivity of $\varepsilon\text{Å} = 4 - j0.0001$ [38]. The PUI for different sliding short

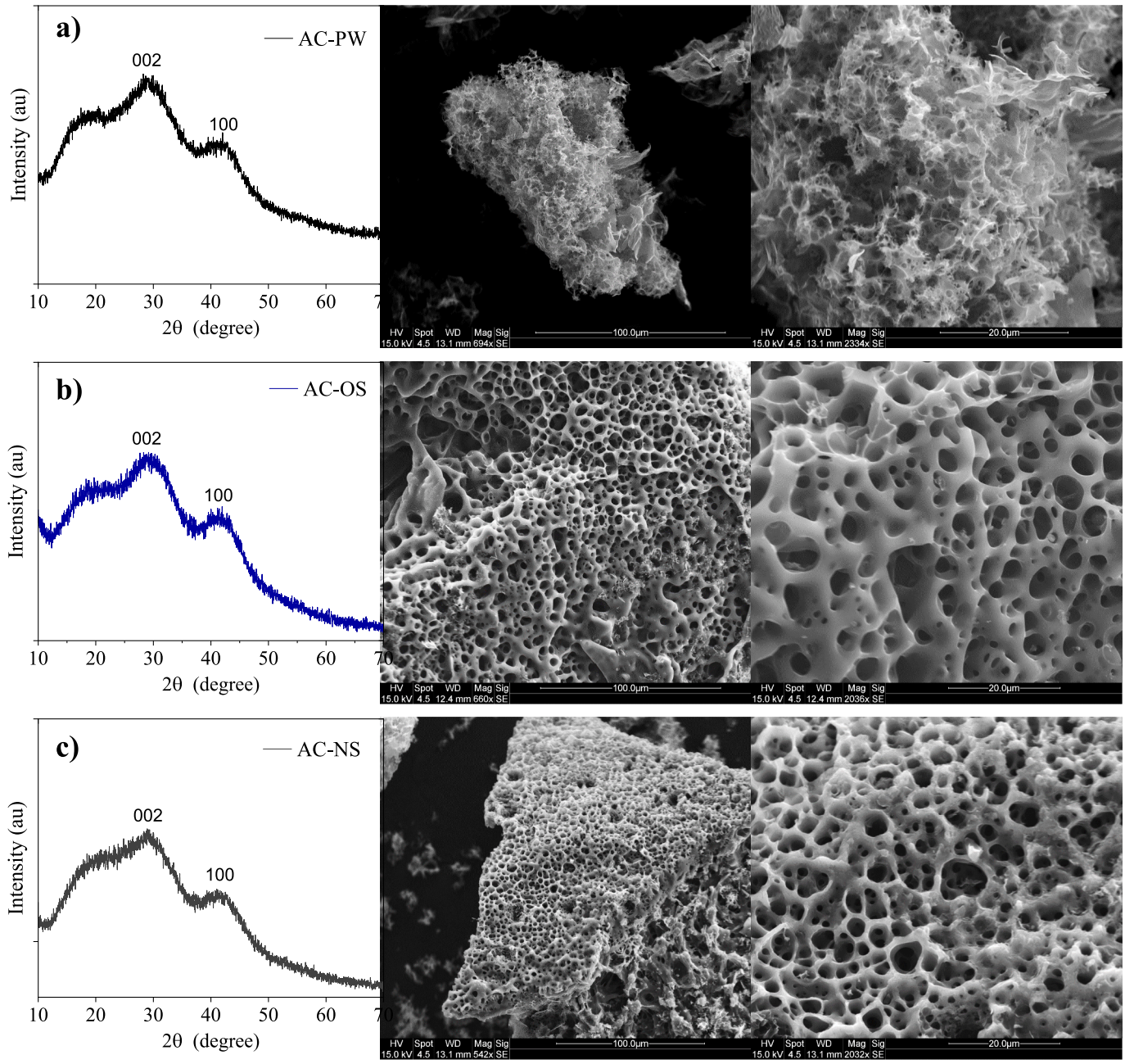

Fig. 9. XRD spectra and SEM images for (a) AC-PW, (b) AC-OS and (c) AC-NS samples.

lengths and sample properties for different temperatures are shown Fig. 4 for an example case of impregnated sample (KOH-PW).

Two operational zones of high uniformity for the full range of properties can be identified around the minimum PUI values on the chart with very small variation in PUI with material properties observed up to 500 °C due to the rather stable dielectric constant across the temperature range. At higher temperatures, the short positioning becomes less relevant regarding treatment uniformity. As the material dielectric properties increase, the minimum and maximum achievable PUI become closer. As the minimum sliding short length is 40 mm (i.e. fully retracted), a sliding short position of 132.5 mm was selected to achieve uniform sample treatment.

To illustrate the difference in treatment uniformity, two cases of the electric field distribution are shown in Fig. 5, for sample properties at 500 °C. In the first case (a), a sliding short length of 102.5 mm was selected, with a PUI of 0.9, representing a low uniformity case. In this case, the fields are mainly concentrated on the left side of the sample, closer to the generator. In the second case (b), a sliding short length of 132.5 mm was used, with a PUI of 0.2, representing a close to optimal uniformity, where the electric fields appear to be more uniformly distributed within the sample, with the maximum at its centre. This analysis highlights the importance of determining a sliding short length in this type of experimental system, as a poor selection can result in uneven heating and localised overheating, which can be accentuated once the sample starts to carbonise.

3.3. *Effect of microwave energy on yield and physicochemical properties of ACs*

The specific microwave energy input required to produce AC by single-step microwave pyrolysis-activation and their respective yields are shown in Table 2, while Fig. 6 shows an example of the microwave

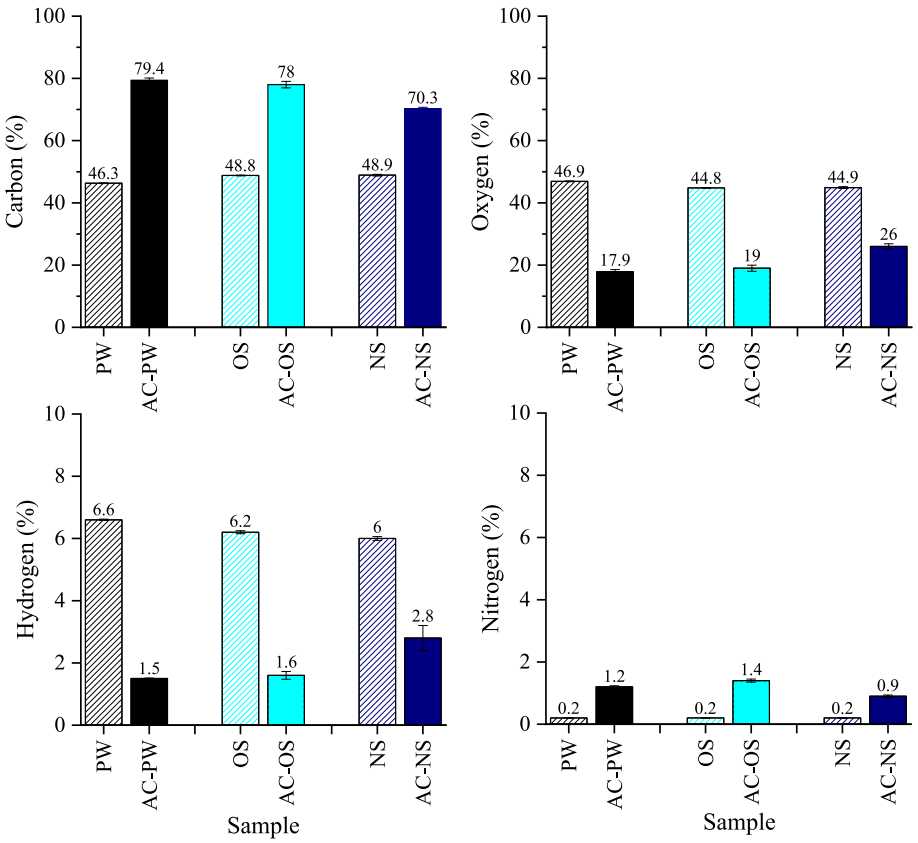

Fig. 10. Elemental composition of raw and AC samples, oxygen calculated by difference.

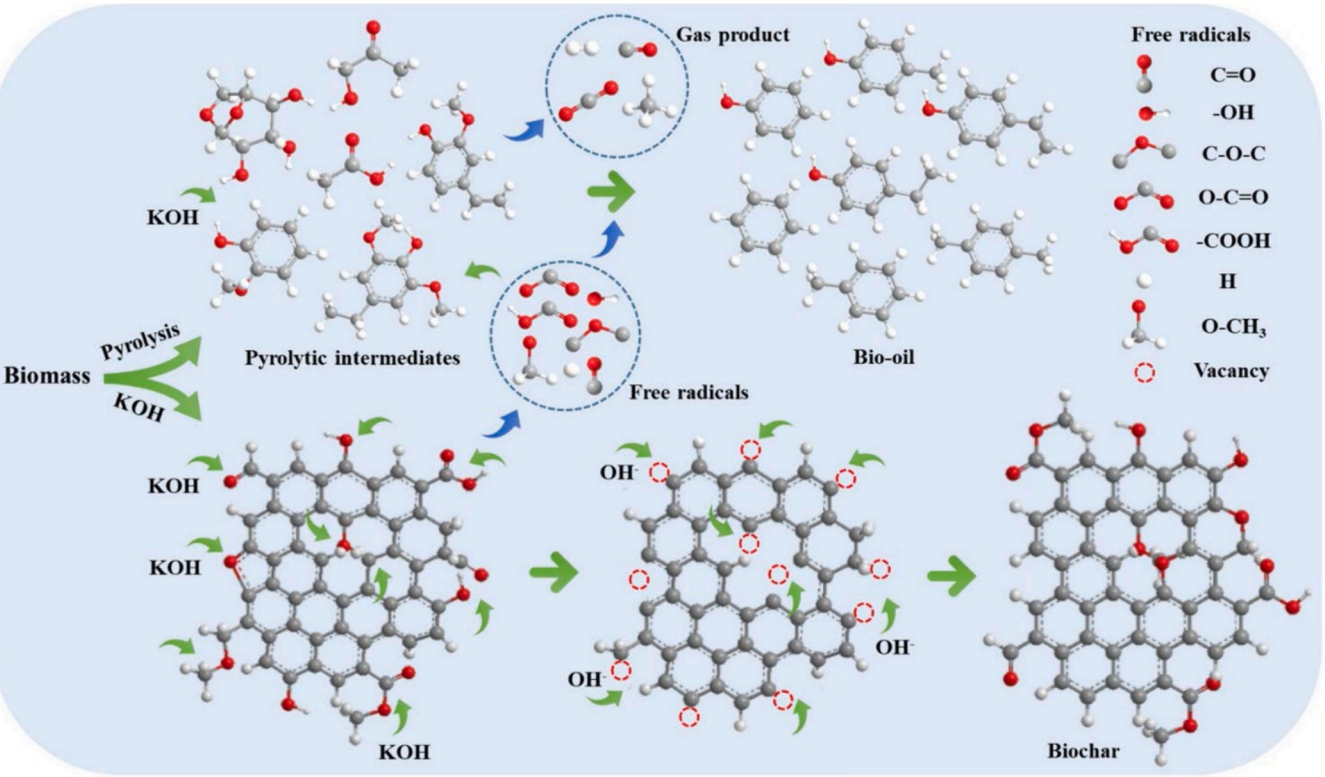

Fig. 11. Chemical reaction pathway of biomass with KOH during pyrolysis. Reused with permission from Elsevier license number 5,803,231,394,606 from [37].

Table 3
Textural parameters of ACs prepared using single-step microwave-pyrolysis.

Sample	S_{BET}	V_{Pore}	$V_{Micropore}$		$V_{Ultra-Micropore}$	
	(m^2/g)	(cm^3/g)	(cm^3/g)	%	(cm^3/g)	%
AC-PW	1,340	0.537	0.487	90.7	0.377	70.3
AC-OS	1,255	0.558	0.451	80.9	0.323	57.9
AC-NS	942	0.407	0.344	84.7	0.249	61.2

power profile for one of the experiments (AC-NS). The energy was efficiently absorbed during the test, representing an average of 95 % adsorbed power with regard to the forward power. This confirms the relevance of characterising and determining the optimum tuner position for the sample position within the microwave applicator to utilize available microwave power and minimize lost energy.

Previous studies indicated that the specific microwave energy influences AC's yield and pore development [4,5]. In general, it was found

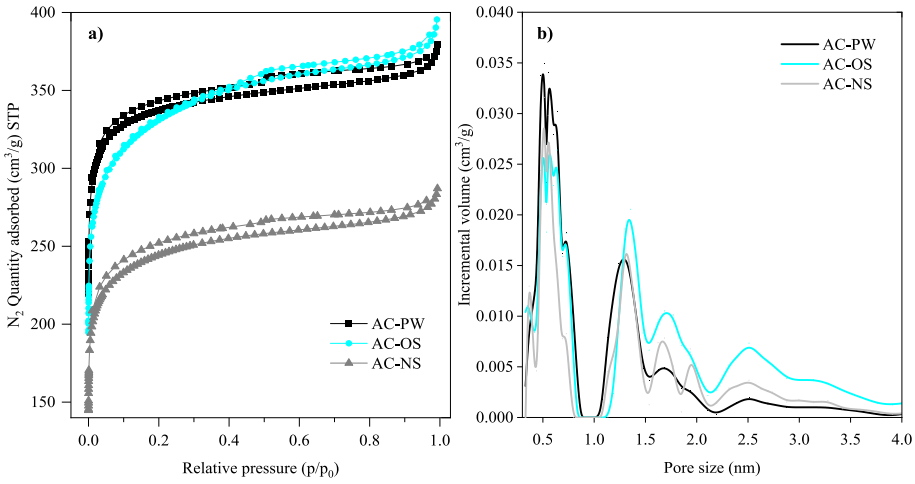

Fig. 12. (a) N_2 adsorption–desorption isotherms at −196 °C and (b) pore size distribution from combined N_2 (−196 °C) and CO_2 (0 °C) of AC.

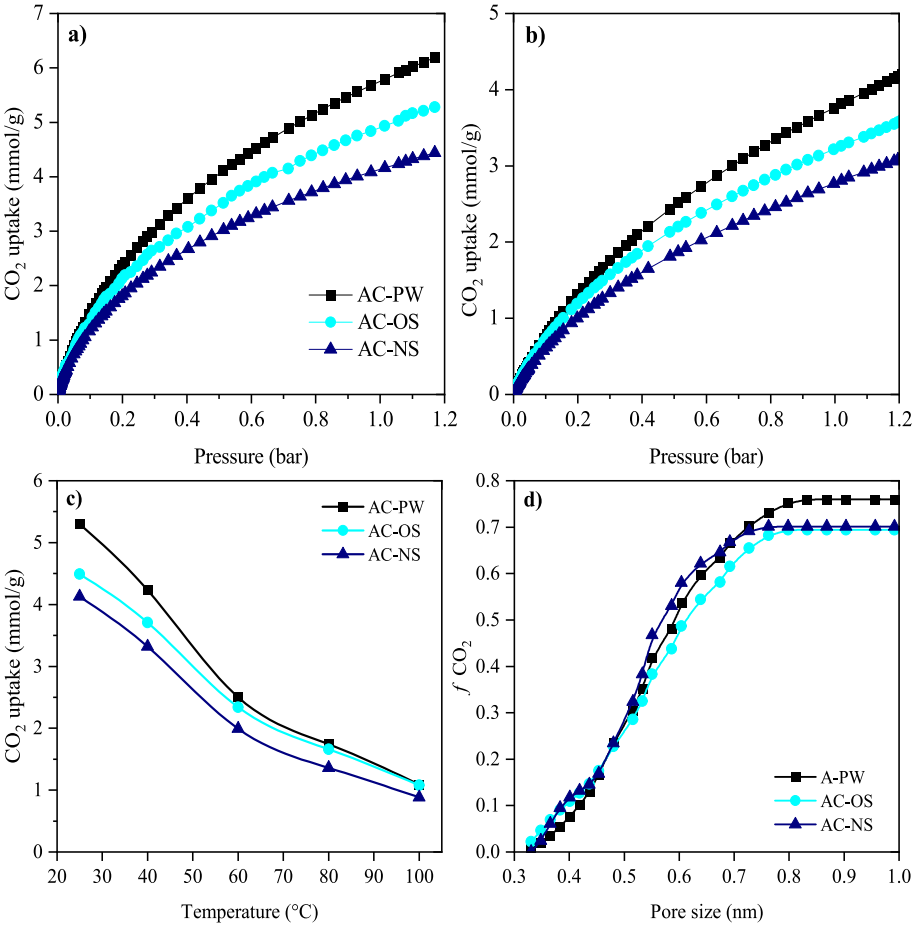

Fig. 13. CO_2 adsorption profiles at (a) 0 °C and (b) 25 °C (conditions: 100 % CO_2, volumetric analysis); (c) CO_2 uptake at different temperatures in a 100 % CO_2 and thermogravimetric method; (d) pore filled by CO_2 with average micropore size of ACs, deduced by applying the NLDFT model to CO_2 isotherms at 0 °C.

Table 4
Comparative CO_2 uptake performance and relationship with textural parameters of activated carbons prepared form different biomass.

Raw material	Carbonisation (**C**) (°C)/time (min) & Activation (**A**) (Temp. °C)/time (min)	Activating Agent	Agent: BiomassAgent:Char ratio	Microwave power / time (W/min)	CO_2 uptake at 1 bar (mmol/g) / T(°C)	S_{BET} (m^2g^{-1})	V_{tot} (cm^3 g^{-1})	V_{micro} (cm^3g^{-1})	Ref.
Pine wood	n/a	KOH	2:1	300/8	6.2/0 °C 4.2/25 °C	1340	0.537	0.487	This work
Olive stones	n/a	KOH	2:1	300/8	5.3/0 °C 3.6/25 °C	1255	0.558	0.451	This work
Pecan nutshell	n/a	KOH	2:1	300/8	4.4/0 °C 3.1/25 °C	941	0.407	0.344	This work
Pecan nutshell	n/a	KOH	1:1	300/6	5.3/0 °C 3.7/25 °C	959	0.377	0.350	[5]
Enteromorpha	C-600/20 A-700/20	KOH	3:1	Variable/20	6/0 °C	1890	0.214	–	[42]
Walnut shells	A-800/60	KOH	1:1	n/a	9.5/0 °C 5.2/25 °C	1868	1.060	0.940	[12]
Chitosan	C-550/120 A-750/60	KOH	–	n/a	3.9/25 °C 5.6/0 °C	1928	–	0.720	[47]
Olive pomace	C-500/15 A-600/30	K_2CO_3	2:1	n/a	3.15/0 °C	582	0.283	0.197	[48]
Corncob	500/120 C-230/480 A-600/60	Melam-KOH	3:1	n/a	3.4/30 °C 4.5/15 °C	1222	0.711	0.620	[16]
Lotus leaf	C-500/60 A-550/60	KOH	2:1	n/a	3.9/25 °C 5.4/0 °C	1487	0.690	0.610	[44]
Rice husk	C-900/60 A-100/60	K_2CO_3-CO_2	5:1	n/a	3.1/25 °C	–	–	–	[2]
Rice husk	A-600/60	KOH	1:1	n/a	3.25/25 °C	536	0.240	0.190	[49]
Chestnut	C-600/120 A-800/120	NH_3	1.25:1	n/a	2.3/25 °C	747	–	–	[50]
Corncob	C-800/180 A-800/180	NH_3-KOH	4:1	n/a	2.8/25 °C	1154	0.570	–	[15]
Empty fruit	C-350/20 A-800/30	KOH	5:1	n/a	3.4/25 °C	1322	0.780	0.23	[43]
Chitosan	A-700/60	KOH	2:3	n/a	6.9/0 °C 4.4/25 °C	1506	0.64	–	[51]

that yield was higher for biomass with lower moisture and ash content i.e. OS>PW>NS. The energy required for completing pyrolysis-activation of samples was 8.6 GJ t^{-1}, and according to textural properties, this energy is sufficient to achieve a developed porous structure in the carbon framework.

Due to the rapid heating rates employed in this study in a single-step of pyrolysis-activation, is fundamental to confirm the complete conversion of impregnated samples to ACs. Fig. S1 (Supplementary Information) shows the TGA of ACs produced have thermal stability across a range of temperatures, with ~10 % mass loss at 600 °C. Additionally, Fig. 7 shows the FT-IR spectra of biomasses and ACs prepared in this study, confirming differences and distinctive peaks characteristics for ACs. The superficial functional groups can be associated to the groups were well-defined peaks. Particularly, the broad peak at ~3400 cm^{-1} could be the O-H stretching of phenols and aldehydes, while the asymmetric stretching of the C-H bond of alkanes, alkenes, and aldehydes could be seen in the range of 2900–3000 cm^{-1}. Additional peaks of relevance can be observed at 1700, 1400–1600 and 1025 cm^{-1}, associated with C=O stretching of carboxylic acids, esters, and ethers, C=C stretching in aromatic structures, and C-O bounds of alcohols [14].

The XPS spectra shown in Fig. 8 were deconvoluted into the main oxygenated groups present in the ACs. The spectra in carboxylic groups (–COOH) was observed in the range of 534.4–535.2 eV. Oxygen in esters and anhydrides (O-C=O/C-O) was identified at 533.4–533.5 eV. Other additional groups found were carbonyl oxygen atoms in anhydrides, esters or hydroxyl groups (O-C=O/OH, 532.2–532.3 eV), carbonyl oxygen (C=O, 531.6–531.8 eV) and adsorbed oxygen (535.3–538.2 eV). Similar surface groups have been reported for AC with KOH [5,37].

The XRD and surface morphology (SEM) of AC are shown in Fig. 9. As can be observed, the AC samples display porous structures with presence of interconnected pores with large conchoidal cavities as a result of the activation process. AC-OS and AC-NS showed visible cavities and pores around the main cell wall structure that was retained after the pyrolysis-activation process. Both ACs were also characterised for higher mechanical resistance. In the case of AC-PW, the cell structure was modified after the pyrolysis-activation process, this could be associated to the nature of PI feedstock, characterised as a soft wood. In this case, the cellulose and lignin could have been destroyed during the activation process, as result of the gasification of carbon structure when reacts with inorganic K. Similar findings have been reported before for AC obtained from Miscanthus and KOH [18]. Is very relevant to mention that highly porous ACs were obtained in a single step in 8 min and all feedstock (PI, OS and NS) showed a hierarchical pore formation from macropores to smaller pores within the framework structure. This parameter is of great relevance in ACs due to enhances the diffusion of CO_2 and the uptake capacity. The XRD diffraction patterns indicate that all the materials are amorphous with low levels of crystallinity. The diffraction patterns show broad peaks at around 25 and 44°, corresponding to the (002) and (100) planes in a non-graphitic disordered carbon structure. Similar diffraction patterns have been observed for activated carbons [39].

The ultimate analysis for biomass and ACs prepared in this study is shown in Fig. 10. It can be observed the single-step microwave pyrolysis-activation allowed the full conversion of biomasses to ACs with carbon content ranging from 70.3 to 79. 4 %. As expected, oxygen and hydrogen content decreased in AC from initial biomass as a result of the pyrolysis-activation process, where hydrogen, carbon monoxide and carbon dioxide evolved [13]. Very important, it was found that PW biomass contains ~46 % of carbon, which increased to 79 % in AC-PW. Hydrogen decreased from 6.6 to 1.5 %, while oxygen decreased from 46.9 to 17.9 %, respectively. Across the AC produced from 3 biomasses, AC-PW was found to have higher increase of carbon and higher decrease of oxygen and hydrogen. These results suggest that the reaction between the KOH and the lignocellulosic matrix of PW was more efficient and promoted higher deoxygenation and dehydrogenation reactions.

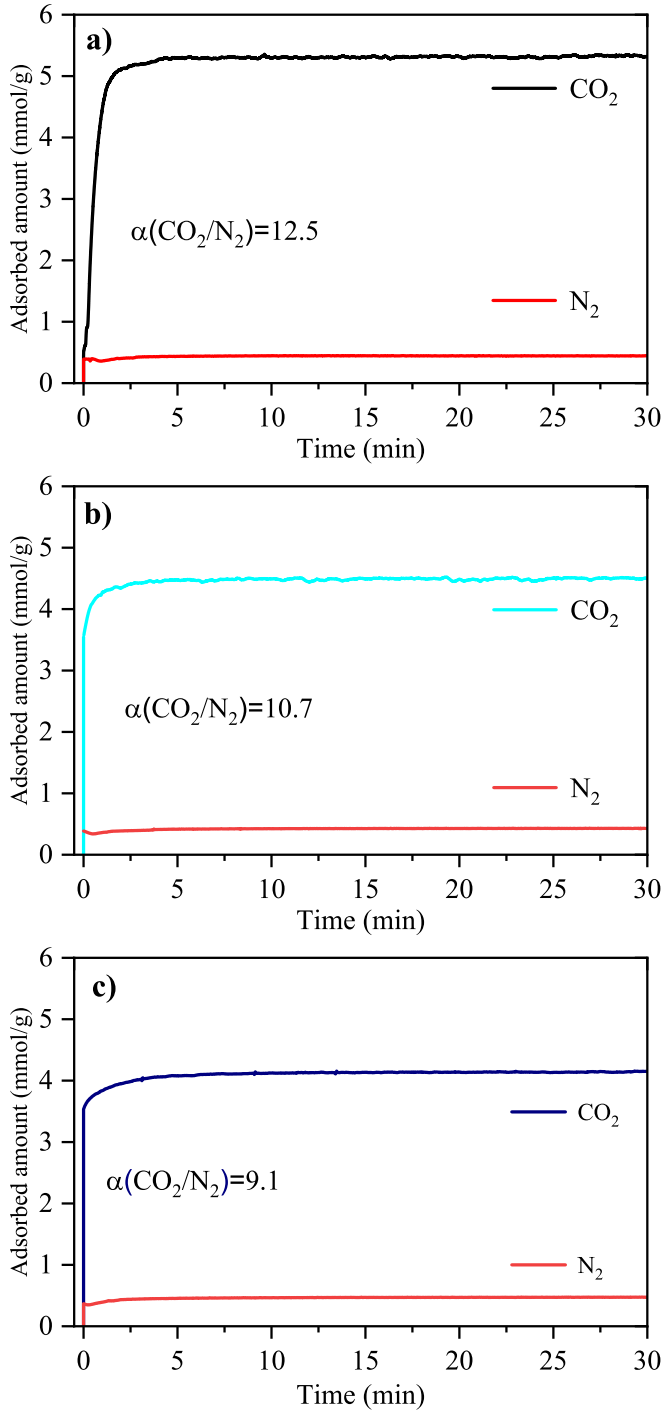

Fig. 14. Adsorption kinetics and selectivity of CO_2 and N_2 (at 25 °C and 1 bar) for (a) AC-PW, (b) AC-OS and (c) AC-NS.

Based on the elemental composition and textural properties, it was found that the reaction between the available oxygenated and hydrogenated groups in PW and KOH enhanced the CO, CO_2 and H_2 gaseous evolution that further enhanced the development of the porous structure. The proposed reaction mechanisms between the PW biomass and KOH and pore formation have been previously reported as detailed in Fig. 11 and reactions below [5,37]:

$$\text{Biomas} + \text{KOH} \rightarrow \text{Biomass.}K_2O + H_2O(l)$$

$$\text{Biomass} + H_2O \rightarrow C + H_2O + \text{tar}$$

$$C + H_2O \rightarrow H_2 + CO$$

$$CO + H_2O \rightarrow H_2 + CO_2$$

$$2K_2O + H_2 + 2CO + C \rightarrow 2C + 2K + H_2O + K_2CO_3$$

$$6KOH + 2C \rightarrow 2K_2CO_3 + 2K + 3H_2$$

$$K_2CO_3 + C \rightarrow K_2O + 2CO$$

$$K_2O + C \rightarrow 2K + CO$$

The comparative textural properties on the effect of biomass feedstock and single microwave-activation step for AC production are shown in Table 3. According to the adsorption–desorption nitrogen isotherms and pore size distribution (Fig. 12), it can be observed that the method proposed in this study is suitable for the porous development in a carbon matrix, independently of the biomass used. According to the classification of IUPAC [40], ACs produced exhibit an isotherm type I and type IV, characteristic of microporous and mesoporous materials. It should be noted that the adsorbed amount at low pressures was significantly higher for AC-PW despite the fact that similar microwave energy was used.

The main characteristic of AC-PW observed is that the pore width peak between 0.33 and 0.6 nm becomes prominent in comparison with the peaks in AC-OS and AC-NS, respectively. Wide pores in AC-OS and AC-NS>2nm) can be observed in Fig. 10b.

The textural properties of the ACs listed in Table 3 show that the specific surface area (S_{BET}) and micropore specific volume are significantly higher for AC-PW, with 1340 m^2/g and 0.48 $cm^3\ g^{-1}$, in comparison to the S_{BET} of 1255 and 942 m^2/g, and V_{mic} of 0.45 and 0.34 for AC-OS and AC-NS, respectively. Results suggest that the production of the surface area and porosity characteristics of ACs are influenced by the nature of the original biomass feedstock [41]. The pyrolysis-activation process involves the softening of the material and release of volatile matter, followed by shrinkage of char. This process allows gas generation, creating small pores within the carbon structure. The DTG curves of biomass in Fig. 3 show that OS and NS have two clear weight loss peaks represented by the shoulder on the weight peak loss. The DTG of PW suggests that hemicellulose and cellulose decomposition occurs at a higher mass loss rate, allowing the enhancement of surface area and pore volume in the structure of AC-PW.

3.4. CO_2 adsorption studies

The CO_2 uptake capacity for all ACs prepared in this study at 0 and 25 °C is shown in Fig. 13. All samples showed significant CO_2 uptake capacity in the range of 4.4 to 6.2 mmol g^{-1} at 0 °C and from 3.1 to 4.1 mmol g^{-1} at 25 °C. AC-PW exhibited the highest CO_2 uptake capacity, followed by AC-OS and AC-NS. Table 4 shows a comparative performance of samples prepared in this study, with previous AC reported in the literature. It is important to note that the CO_2 uptake of samples produced in this study showed comparable or even higher performance to activated carbons prepared using conventional heating method (See Table 4). It can be observed that these materials were prepared in two steps of carbonization (C) followed by activation (A) at high temperatures and longer processing times (>60 min) compared to microwaves (8 min). Luo et al. [42] reported the combination of conventional and microwave heating where Enteromorpha biomass was firstly carbonised and activated using a KOH:char ratio of 3:1. The sample was subjected to microwaves adjusting power to achieve 700C for 20 min. The CO_2 uptake reported was 6 mmol g^{-1} which is comparable to the uptake reported by AC-PW. It should be noted that the AC-PW was prepared in a single-step, using lower KOH ratio and lower processing time (8 min).

Parshetti et al. [43] used carbonisation followed by activation of empty fruit char (5:1 KOH:char ratio), while Li et al. [44] followed

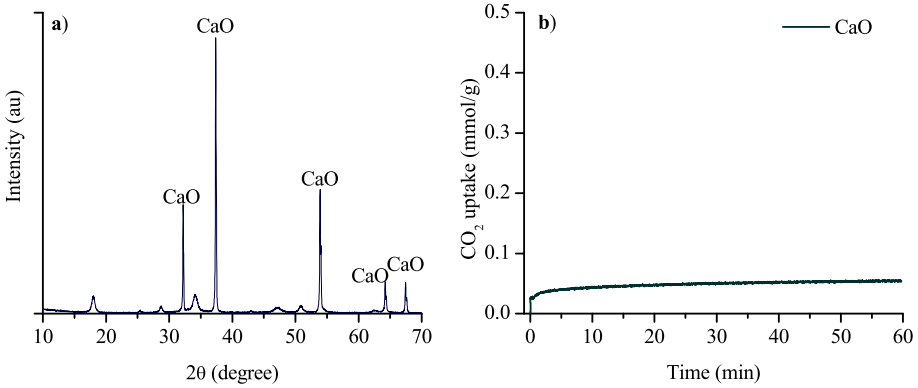

Fig. 15. XRD of inorganic matter (ash) of sample AC-NS (a) and CO_2 uptake (b). Conditions: 100 % CO_2, 25 °C, 1 bar.

similar approach using Lotus leaf and KOH:char ratio of 2:1. In both studies, maximum CO_2 uptake was 3.4 (at 25 °C) and 5.4 mmol g^{-1}. Corncob performance was reported by Geng et al. [15] using AC produced by NH3-KOH activation at 4:1 ratio. Maximum CO_2 uptake was 2.8 mmol g^{-1} at 25 °C. Similarly, corncob AC performance was studied by Sarwar et al. [16]. In this case, AC was produced by two stages of carbonisation and activation using melamine and KOH at 3:1 ratio. The CO_2 uptake reported was 4.5 mmol g^{-1} at 15 °C. Results show that the biomasses evaluated in this study are suitable for the preparation of ACs and for CO_2 capture and that microwave heating has great potential in biomass processing due to offering desired properties in ACs produced in a simpler, faster and more sustainable approach that the traditional conventional synthesis process. It should be noted that this approach confirms that there is no requirement for multiple steps in microwave heating, as reported before [42]. The pyrolytic gases involved in the decomposition of biomass could play a favourable role in the development of porous structure, in addition to the activation with KOH.

This study confirms that not only the surface area and volume of pores are relevant for high CO_2 uptake, but also the ultra-micropores. In this regard, 70.3 % of the total pore volume present in AC-PW corresponds to pores of <0.8 nm, compared with 57.9 % in AC-OS and 61.2 % for AC-NS. The contribution of these ultra-micropores to the CO_2 uptake capacity is evidenced in Fig. 13d). The fraction of ultra-micropore filling ($f_{CO2} = CO_{2uptake}/(V_{mic} \cdot \rho_{CO2,}$) describes the ratio of pore filled by CO_2 as a fraction of pore size in the material [5]. The results indicate the highest fraction of filled pores occurs in pores of the size of 0.8 nm, whereas other pores, such as super-micropores (0.8–2 nm) are not relevant for CO_2 capture at the given conditions (0)–(1) bar). The CO_2 uptake is negligible for micropores widths larger than around two to three times the molecular diameter (CO_2 diameter ~ 0.33 nm); therefore, the optimum pore size is between 0.7 and 0.9 nm, but micropores of 0.8–2 nm may become relevant for enhanced CO_2 capture at higher pressures (>30 bar). Wide pores in ACs such as mesopores (2–5 nm) are relevant in the CO_2 uptake mechanisms due to facilitating mass diffusion of gas molecules to ultra-micropores, confirming hierarchical carbon structures (mesopores and micropores and ultra-micropores) are necessary to mitigate transport restrictions for CO_2 capture [45]. In post-combustion, CO_2 capture is fundamental to determining the performance of materials in a range of relevant temperatures. As depicted in Fig. 13c), as temperature increases, the uptake decreases as a result of the greater energy of CO_2 molecules that can escape from the surface rapidly. Similar results have been reported in the literature [46].

3.4.1. Adsorption kinetics and selectivity

The adsorption kinetics of CO_2 reached the maximum adsorption capacity within 5 min, confirming a low mass transfer resistance over the activated carbons (see Fig. 14). The low time required to reach the equilibrium may be associated with the optimum pore size of carbon structure, but to the large surface area displayed by the materials. The selectivity and adsorption capacity followed the order AC-NS<AC-OS<AC-PW, which is directly related to the textural properties and surface chemical characteristics. The surface chemistry of activated carbon, originated by superficial functional groups such as nitrogen-containing groups, and basicity nature due to the resonation of π-electrons present in carbon aromatic rings, can improve the selectivity of the activated carbon materials and the hydrophobicity nature of the activated carbons. The influence of inorganic matter (calcium oxide (CaO)) was investigated for the AC-NS, due to its higher content of ash. Results confirm that the ash has little contribution to the overall CO_2 uptake performance, as can be observed in Fig. 15.

3.4.2. Adsorbents reuse and CO_2 adsorption cycles

The regeneration performance of ACs is essential to evaluate applications at large scale. Fig. 16 shows the cyclic CO_2 adsorption–desorption properties of materials prepared in this study. From results in kinetics studies, CO_2 adsorption was evaluated at 25 °C, 1 bar and equilibrium time of 5 min. The results highlight that CO_2 adsorption capacity continues unchanged after 15 cycles, maintaining >98 % capacity. This suggests the main adsorption mechanism is physisorption, where the desorption of CO_2 is simple and reversible in nature. The results show that AC-PW, AC-OS and AC-NS have high reuse capability, which is fundamental for large scale applications.

3.4.3. Isosteric heat of adsorption

The interaction strength between the CO_2 and the ACs was determined by the isosteric heat of adsorption (Q_{st}). These were calculated via the CO_2 adsorption isotherms at 0 and 25 °C and by applying the Clausius-Clapeyron equation. The Q_{st} values are comparable with previously reported values for porous carbons [52,53]. Results shown in Fig. 17 highlight that all ACs exhibit high Q_{st} of 26–29 kJ/mol at low CO_2 uptake due to the available ultra-microporosity on the ACs which is known to increase the heat of adsorption. At higher CO_2 uptake capacities, Q_{st} decreased; this may be attributed to increasing in surface coverage because of stronger interactions between oxygenated functional groups and the CO_2 molecules. A higher Q_{st} of 29 kJ/mol was obtained for sample AC-OS in comparison with AC-PI and AC-NS, indicating a stronger interaction between the CO_2 molecule and AC-OS surface occurs. This could be associated with the surface chemistry. In particular, AC-OS contains larger content of nitrogen, which was also evidenced in the elemental analysis and XPS results. Wide XPS scan showed a clear N 1s peak only present for AC-OS sample (Supplementary Information). It has been reported that nitrogen functional groups on the AC can enhance electron donor properties of carbon by influencing the carbon spin density, and therefore increasing the Q_{st} [51].

The Q_{st} values reported for ACs prepared in this study, are lower than the values reported for chemisorption (<40 kJ/mol)[54], indicating weak forces between the adsorbent surface and CO_2, and that CO_2 uptake occurs as result of mechanisms of physical adsorption and,

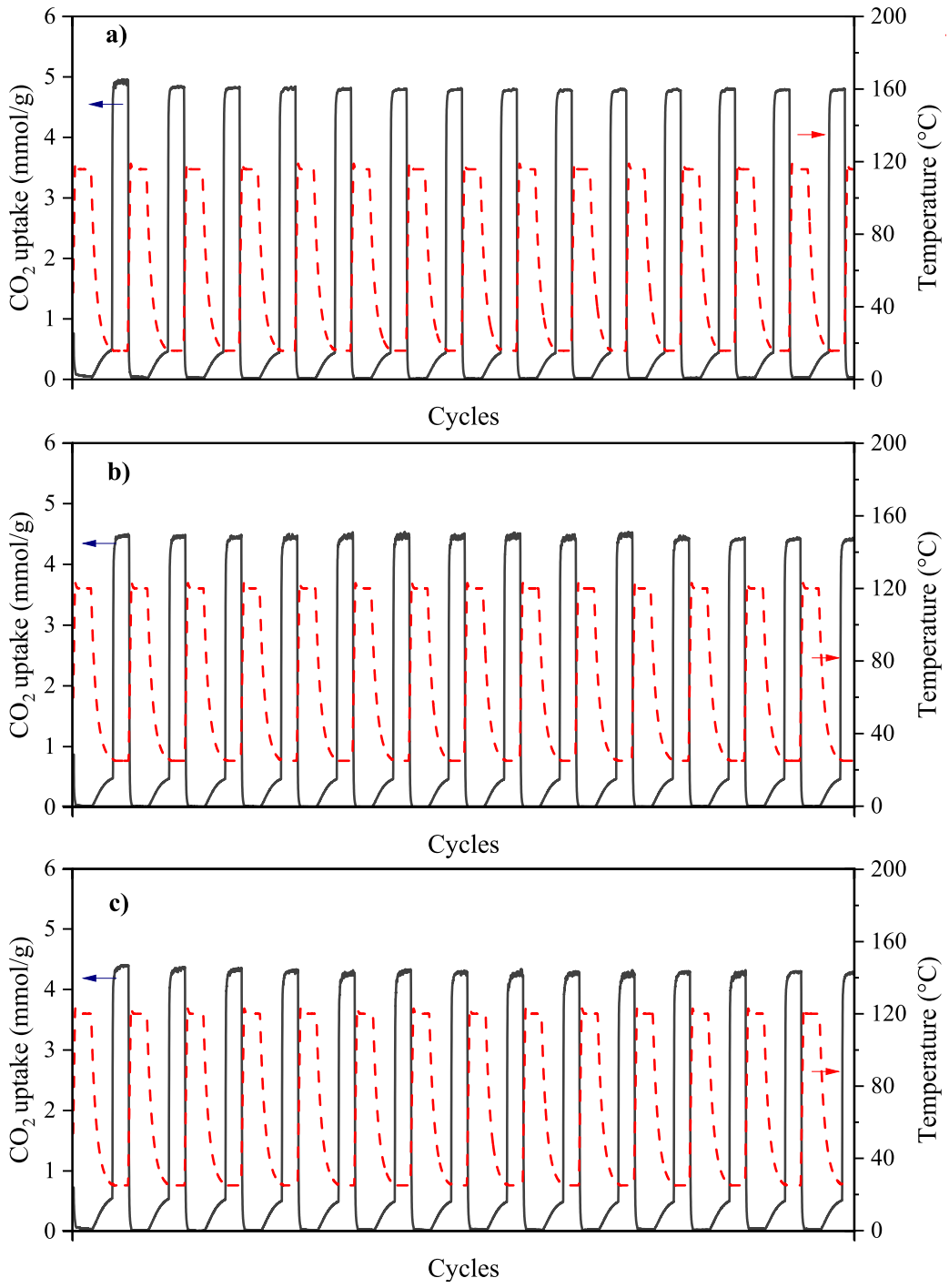

Fig. 16. Cyclic CO_2 adsorption performance of AC-PW (a), AC-OS (B) and AC-NS (c) activated carbons. Thermogravimetric CO_2 adsorption at 1 bar and 25 °C.

therefore, confirming that is a reversible process with fast regeneration rates (See Fig. 16).

4. Conclusions

This study demonstrated the potential of biomass residues, specifically pine wood, olive stones, and pecan nutshells, as effective feedstocks for producing activated carbons (ACs) using a rapid, low-energy microwave-assisted pyrolysis-activation process. Among the material evaluated, pine wood activated carbon displayed superior performance for CO_2 capture due to its large surface area and ultra-microporosity, which also resulted in fast kinetic of adsorption, greater selectivity and recyclability. Dielectric characterisation and electromagnetic simulations confirmed the relevance of characterising the feedstock and microwave applicator system. This study demonstrated single-step microwave pyrolysis-activation method is a promising approach for biomass reutilisation and AC production. Due to the reduction of time, elimination of pre-conditioning and chemical agents involved in the synthesis, this method stands as a sustainable approach that could play a crucial role addressing the biomass residues valorisation and climate change challenges by developing advanced materials for CO_2 capture.

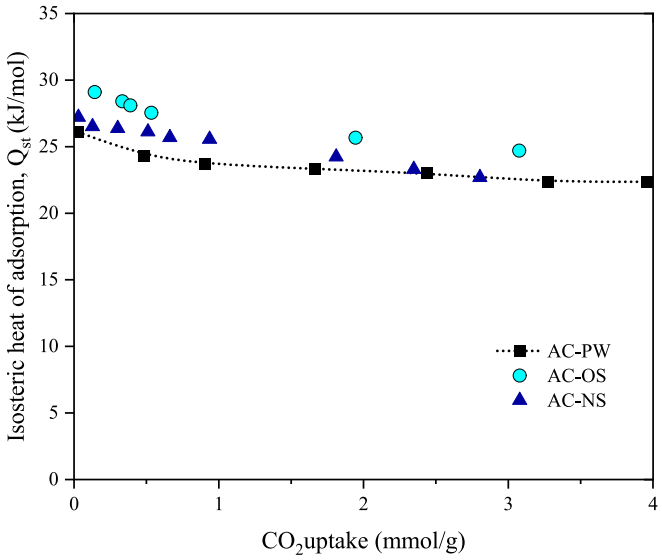

Fig. 17. Isosteric heat of CO_2 adsorption for all AC prepared in this study at different CO_2 uptakes.

CRediT authorship contribution statement

Gabriela Duran-Jimenez: Writing – original draft, Methodology, Investigation, Funding acquisition, Conceptualization. **Jose Rodriguez:** Writing – review & editing, Validation, Investigation. **Lee Stevens:** Writing – review & editing, Validation, Investigation. **Sanad Altarawneh:** Writing – review & editing, Validation, Investigation. **Andrew Batchelor:** Writing – review & editing, Validation, Investigation. **Long Jiang:** Data curation, Formal analysis. **Chris Dodds:** Writing – review & editing, Validation.

Declaration of competing interest

The authors declare that they have no known competing financial interests or personal relationships that could have appeared to influence the work reported in this paper.

Data availability

Data will be made available on request.

Acknowledgements

The authors are grateful to Matt Nicholls for providing support in commissioning the microwave system and the Nanoscale and Microscale Research Centre (nmRC) University of Nottingham for the support with XPS.

Appendix A. Supplementary data

Supplementary data to this article can be found online at https://doi.org/10.1016/j.cej.2024.156135.

References

[1] M.N. Anwar, A. Fayyaz, N.F. Sohail, M.F. Khokhar, M. Baqar, W.D. Khan, K. Rasool, M. Rehan, A.S. Nizami, CO_2 capture and storage: a way forward for sustainable environment, J. Environ. Manage. 226 (2018) 131–144, https://doi.org/10.1016/j.jenvman.2018.08.009.

[2] M. Li, R. Xiao, Preparation of a dual pore structure activated carbon from rice husk char as an adsorbent for CO_2 capture, Fuel Process. Technol. 186 (2019) 35–39, https://doi.org/10.1016/j.fuproc.2018.12.015.

[3] N. Höhne, M.J. Gidden, M. den Elzen, F. Hans, C. Fyson, A. Geiges, M.L. Jeffery, S. Gonzales-Zuñiga, S. Mooldijk, W. Hare, J. Rogelj, Wave of net zero emission targets opens window to meeting the Paris Agreement, Nat. Clim. Chang. 11 (2021) 820–822, https://doi.org/10.1038/s41558-021-01142-2.

[4] G. Durán-Jiménez, E.T. Kostas, L.A. Stevens, W. Meredith, M. Erans, V. Hernández-Montoya, A. Buttress, C.N. Uguna, E. Binner, Green and simple approach for low-cost bioproducts preparation and CO_2 capture, Chemosphere 279 (2021), https://doi.org/10.1016/j.chemosphere.2021.130512.

[5] G. Durán-Jiménez, L.A. Stevens, E.T. Kostas, V. Hernández-Montoya, J. P. Robinson, E.R. Binner, Rapid, simple and sustainable synthesis of ultra-microporous carbons with high performance for CO_2 uptake, via microwave heating, Chem. Eng. J. 388 (2020), https://doi.org/10.1016/j.cej.2020.124309.

[6] X. Ren, M. Shanb Ghazani, H. Zhu, W. Ao, H. Zhang, E. Moreside, J. Zhu, P. Yang, N. Zhong, X. Bi, Challenges and opportunities in microwave-assisted catalytic pyrolysis of biomass: a review, Appl. Energy 315 (2022) 118970, https://doi.org/10.1016/j.apenergy.2022.118970.

[7] Y. Gao, J. Remón, A.S. Matharu, Microwave-assisted hydrothermal treatments for biomass valorisation: a critical review, Green Chem. 23 (2021) 3502–3525, https://doi.org/10.1039/D1GC00623A.

[8] A.A. Arpia, W.-H. Chen, S.S. Lam, P. Rousset, M.D.G. de Luna, Sustainable biofuel and bioenergy production from biomass waste residues using microwave-assisted heating: a comprehensive review, Chem. Eng. J. 403 (2021) 126233, https://doi.org/10.1016/j.cej.2020.126233.

[9] H. Li, V.L. Budarin, J.H. Clark, M. North, X. Wu, Rapid and efficient adsorption of methylene blue dye from aqueous solution by hierarchically porous, activated starbons®: mechanism and porosity dependence, J. Hazard. Mater. 436 (2022) 129174, https://doi.org/10.1016/j.jhazmat.2022.129174.

[10] G. Durán-Jiménez, V. Hernández-Montoya, M.A. Montes-Morán, A. Bonilla-Petriciolet, N.A. Rangel-Vázquez, Adsorption of dyes with different molecular properties on activated carbons prepared from lignocellulosic wastes by Taguchi method, Microporous Mesoporous Mater. 199 (2014) 99–107, https://doi.org/10.1016/j.micromeso.2014.08.013.

[11] G. Durán-Jiménez, J. Rodriguez, E.T. Kostas, L.A. Stevens, L. Lozada-Rodríguez, E. Binner, C. Dodds, Simultaneous conventional and microwave heating for the synthesis of adsorbents for CO_2 capture: comparative study to pristine technologies, Chem. Eng. J. 438 (2022), https://doi.org/10.1016/j.cej.2022.135549.

[12] J. Serafin, B. Dziejarski, O.F. Cruz Junior, J. Sreńscek-Nazzal, Design of highly microporous activated carbons based on walnut shell biomass for H_2 and CO_2 storage, Carbon N. Y. 201 (2023) 633–647, https://doi.org/10.1016/j.carbon.2022.09.013.

[13] J.M. Illingworth, B. Rand, P.T. Williams, Understanding the mechanism of two-step, pyrolysis-alkali chemical activation of fibrous biomass for the production of activated carbon fibre matting, Fuel Process. Technol. 235 (2022) 107348, https://doi.org/10.1016/j.fuproc.2022.107348.

[14] G. Durán-Jiménez, J. Rodriguez, L. Stevens, E.T. Kostas, C. Dodds, Microwave pyrolysis of waste biomass and synthesis of micro-mesoporous activated carbons: the role of textural properties for CO_2 and textile dye adsorption, Chem. Eng. J. 488 (2024), https://doi.org/10.1016/j.cej.2024.150926.

[15] Z. Geng, Q. Xiao, H. Lv, B. Li, H. Wu, Y. Lu, C. Zhang, One-step synthesis of microporous carbon monoliths derived from biomass with high nitrogen doping content for highly selective CO_2 capture, Sci. Rep. 6 (2016) 30049, https://doi.org/10.1038/srep30049.

[16] A. Sarwar, M. Ali, A.H. Khoja, A. Nawar, A. Waqas, R. Liaquat, S.R. Naqvi, M. Asjid, Synthesis and characterization of biomass-derived surface-modified activated carbon for enhanced CO_2 adsorption, J. CO_2 Util. 46 (2021) 101476, https://doi.org/10.1016/j.jcou.2021.101476.

[17] M.R. Ketabchi, S. Babamohammadi, W.G. Davies, M. Gorbounov, S. Masoudi Soltani, Latest advances and challenges in carbon capture using bio-based sorbents: a state-of-the-art review, Carbon Capture Sci. Technol. 6 (2023), https://doi.org/10.1016/j.ccst.2022.100087.

[18] O. Oginni, K. Singh, G. Oporto, B. Dawson-Andoh, L. McDonald, E. Sabolsky, Influence of one-step and two-step KOH activation on activated carbon characteristics, Bioresour. Technol. Rep. 7 (2019), https://doi.org/10.1016/j.biteb.2019.100266.

[19] A. Zubrik, M. Matik, S. Hredzák, M. Lovás, Z. Danková, M. Kováčová, J. Briančin, Preparation of chemically activated carbon from waste biomass by single-stage and two-stage pyrolysis, J. Clean. Prod. 143 (2017) 643–653, https://doi.org/10.1016/j.jclepro.2016.12.061.

[20] M. Adam, D. Beneroso, J. Katrib, S. Kingman, J.P. Robinson, Microwave fluidized bed for biomass pyrolysis. Part I: process design, Biofuels Bioproducts Biorefining 11 (2017) 601–612, https://doi.org/10.1002/bbb.1780.

[21] M. Adam, D. Beneroso, J. Katrib, S. Kingman, J.P. Robinson, Microwave fluidized bed for biomass pyrolysis. Part II: effect of process parameters, Biofuels Bioproducts Biorefining 11 (2017) 613–624, https://doi.org/10.1002/bbb.1781.

[22] D. Beneroso, T. Monti, E.T. Kostas, J. Robinson, Microwave pyrolysis of biomass for bio-oil production: Scalable processing concepts, Chem. Eng. J. 316 (2017) 481–498, https://doi.org/10.1016/j.cej.2017.01.130.

[23] D.V. Suriapparao, H.K. Tanneru, B.R. Reddy, A review on the role of susceptors in the recovery of valuable renewable carbon products from microwave-assisted pyrolysis of lignocellulosic and algal biomasses: prospects and challenges, Environ. Res. 215 (2022), https://doi.org/10.1016/j.envres.2022.114378.

[24] A.K. Silos-Llamas, H. Sudibyo, V. Hernández-Montoya, W. Meredith, G. Durán-Jiménez, Fast pyrolysis of agricultural residues: reaction mechanisms and effects of feedstock properties and microwave operating conditions on the yield and product composition, J. Anal. Appl. Pyrol. 175 (2023), https://doi.org/10.1016/j.jaap.2023.106217.

[25] E.T. Kostas, G. Durán-Jiménez, B.J. Shepherd, W. Meredith, L.A. Stevens, O.S. A. Williams, G.J. Lye, J.P. Robinson, Microwave pyrolysis of olive pomace for bio-oil and bio-char production, Chem. Eng. J. 387 (2020), https://doi.org/10.1016/j.cej.2019.123404.
[26] M. Mariana, E.M. Mistar, T. Alfatah, M.D. Supardan, High-porous activated carbon derived from Myristica fragrans shell using one-step KOH activation for methylene blue adsorption, Bioresour. Technol. Rep. 16 (2021), https://doi.org/10.1016/j.biteb.2021.100845.
[27] E.M. Mistar, T. Alfatah, M.D. Supardan, Synthesis and characterization of activated carbon from Bambusa vulgaris striata using two-step KOH activation, J. Mater. Res. Technol. 9 (2020) 6278–6286, https://doi.org/10.1016/j.jmrt.2020.03.041.
[28] J. Rodriguez, J. Ampuero, W. Valderrama, A. Buttress, C. Dodds, S. Kingman, H. Carrasco, S-band elliptical–cylindrical cavity resonator for material processing, Microw. Opt. Technol. Lett. 64 (2022) 2160–2164, https://doi.org/10.1002/mop.33431.
[29] G. Durán-Jiménez, V. Hernández-Montoya, J. Rodríguez Oyarzun, M.Á. Montes-Morán, E. Binner, Pb(II) removal using carbon adsorbents prepared by hybrid heating system: Understanding the microwave heating by dielectric characterization and numerical simulation, J. Mol. Liq. 277 (2019) 663–671, https://doi.org/10.1016/j.molliq.2018.12.143.
[30] J. Sun, W. Wang, Q. Yue, Review on microwave-matter interaction fundamentals and efficient microwave-associated heating strategies, Materials 9 (2016), https://doi.org/10.3390/ma9040231.
[31] W. Ao, J. Fu, X. Mao, Q. Kang, C. Ran, Y. Liu, H. Zhang, Z. Gao, J. Li, G. Liu, J. Dai, Microwave assisted preparation of activated carbon from biomass: a review, Renew. Sustain. Energy Rev. 92 (2018) 958–979, https://doi.org/10.1016/j.rser.2018.04.051.
[32] O. Baytar, Ö. Şahin, C. Saka, Sequential application of microwave and conventional heating methods for preparation of activated carbon from biomass and its methylene blue adsorption, Appl. Therm. Eng. 138 (2018) 542–551, https://doi.org/10.1016/j.applthermaleng.2018.04.039.
[33] A. Parkash, J.K. Vaid, A. Mansingh, Measurement of dielectric parameters at microwave frequencies by cavity-perturbation technique, IEEE Trans. Microw. Theory Tech. 27 (1979) 791–795, https://doi.org/10.1109/TMTT.1979.1129731.
[34] COMSOL Multiphysics(r) v. 6.2., The RF Module User's Guide, Stockholm, Sweden, 2023. www.comsol.com/blogs.
[35] G. Tiwari, S. Wang, J. Tang, S.L. Birla, Analysis of radio frequency (RF) power distribution in dry food materials, J. Food Eng. 104 (2011) 548–556, https://doi.org/10.1016/j.jfoodeng.2011.01.015.
[36] G. Duran-Jimenez, T. Monti, J.J. Titman, V. Hernandez-Montoya, S.W. Kingman, E. R. Binner, New insights into microwave pyrolysis of biomass: preparation of carbon-based products from pecan nutshells and their application in wastewater treatment, J. Anal. Appl. Pyrol. 124 (2017) 113–121, https://doi.org/10.1016/j.jaap.2017.02.013.
[37] W. Chen, M. Gong, K. Li, M. Xia, Z. Chen, H. Xiao, Y. Fang, Y. Chen, H. Yang, H. Chen, Insight into KOH activation mechanism during biomass pyrolysis: chemical reactions between O-containing groups and KOH, Appl. Energy 278 (2020), https://doi.org/10.1016/j.apenergy.2020.115730.
[38] A.J. Buttress, J.M. Rodriguez, A. Ure, R.S. Ferrari, C. Dodds, S.W. Kingman, Production of high purity silica by microfluidic-inclusion fracture using microwave pre-treatment, Miner. Eng. 131 (2019) 407–419, https://doi.org/10.1016/j.mineng.2018.11.025.
[39] A. Sarwar, M. Ali, A.H. Khoja, A. Nawar, A. Waqas, R. Liaquat, S.R. Naqvi, M. Asjid, Synthesis and characterization of biomass-derived surface-modified activated carbon for enhanced CO_2 adsorption, J. CO_2 Util. 46 (2021), https://doi.org/10.1016/j.jcou.2021.101476.
[40] M. Thommes, K. Kaneko, A.V. Neimark, J.P. Olivier, F. Rodriguez-Reinoso, J. Rouquerol, K.S.W. Sing, Physisorption of gases, with special reference to the evaluation of surface area and pore size distribution (IUPAC Technical Report), Pure Appl. Chem. 87 (2015) 1051–1069, https://doi.org/10.1515/pac-2014-1117.
[41] A.R. Reed, P.T. Williams, Thermal processing of biomass natural fibre wastes by pyrolysis, Int. J. Energy Res. 28 (2004) 131–145, https://doi.org/10.1002/er.956.
[42] J. Luo, Y. Chen, H. Huang, R. Ma, N. Ma, F. Yan, J. Xu, J. Zhang, J. Chen, S. Sun, Microwave-coordinated KOH directionally modulated N/O co-doped porous biochar from Enteromorpha and its structure–effect relationships in efficient CO_2 capture, Chem. Eng. J. 473 (2023) 145279, https://doi.org/10.1016/j.cej.2023.145279.
[43] G.K. Parshetti, S. Chowdhury, R. Balasubramanian, Biomass derived low-cost microporous adsorbents for efficient CO_2 capture, Fuel 148 (2015) 246–254, https://doi.org/10.1016/j.fuel.2015.01.032.
[44] Q. Li, S. Liu, L. Wang, F. Chen, J. Shao, X. Hu, Efficient nitrogen doped porous carbonaceous CO_2 adsorbents based on lotus leaf, J. Environ. Sci. 103 (2021) 268–278, https://doi.org/10.1016/j.jes.2020.11.008.
[45] A. Rehman, Y.-J. Heo, G. Nazir, S.-J. Park, Solvent-free, one-pot synthesis of nitrogen-tailored alkali-activated microporous carbons with an efficient CO_2 adsorption, Carbon N. Y. 172 (2021) 71–82, https://doi.org/10.1016/j.carbon.2020.09.088.
[46] U. Kamran, S.-J. Park, Chemically modified carbonaceous adsorbents for enhanced CO_2 capture: a review, J. Clean. Prod. 290 (2021) 125776, https://doi.org/10.1016/j.jclepro.2020.125776.
[47] J. Li, A. Bao, J. Chen, Y. Bao, A green route to CO_2 adsorption on biomass chitosan derived nitrogen-doped micropore-dominated carbon nanosheets by different activators, J. Environ. Chem. Eng. 10 (2022) 107021, https://doi.org/10.1016/j.jece.2021.107021.
[48] K. Kiełbasa, Ş. Bayar, E.A. Varol, J. Sreńscek-Nazzal, M. Bosacka, B. Michalkiewicz, Thermochemical conversion of lignocellulosic biomass - olive pomace - into activated biocarbon for CO_2 adsorption, Ind. Crop. Prod. 187 (2022) 115416, https://doi.org/10.1016/j.indcrop.2022.115416.
[49] X. Liu, Y. Sun, J. Liu, C. Sun, H. Liu, Q. Xue, E. Smith, C. Snape, Potassium and zeolitic structure modified ultra-microporous adsorbent materials from a renewable feedstock with favorable surface chemistry for CO_2 capture, ACS Appl. Mater. Interfaces 9 (2017) 26826–26839, https://doi.org/10.1021/acsami.7b06665.
[50] K.M. Nelson, S.M. Mahurin, R.T. Mayes, B. Williamson, C.M. Teague, A.J. Binder, L. Baggetto, G.M. Veith, S. Dai, Preparation and CO_2 adsorption properties of soft-templated mesoporous carbons derived from chestnut tannin precursors, Microporous Mesoporous Mater. 222 (2016) 94–103, https://doi.org/10.1016/j.micromeso.2015.09.050.
[51] J. Shao, J. Wang, Q. Yu, F. Yang, M. Demir, O.C. Altinci, A. Umay, L. Wang, X. Hu, Unlocking the potential of N-doped porous Carbon: facile synthesis and superior CO_2 adsorption performance, Sep. Purif. Technol. 333 (2024), https://doi.org/10.1016/j.seppur.2023.125891.
[52] Gautam, S. Sahoo, Experimental investigation on different activated carbons as adsorbents for CO_2 capture, Therm. Sci. Eng. Prog. 33 (2022), https://doi.org/10.1016/j.tsep.2022.101339.
[53] S. Wang, Y.R. Lee, Y. Won, H. Kim, S.E. Jeong, B. Wook Hwang, A. Ra Cho, J. Y. Kim, Y. Cheol Park, H. Nam, D.H. Lee, H. Kim, S.H. Jo, Development of high-performance adsorbent using KOH-impregnated rice husk-based activated carbon for indoor CO_2 adsorption, Chem. Eng. J. 437 (2022), https://doi.org/10.1016/j.cej.2022.135378.
[54] B. Kaur, J. Singh, R.K. Gupta, H. Bhunia, Porous carbons derived from polyethylene terephthalate (PET) waste for CO_2 capture studies, J. Environ. Manage. 242 (2019) 68–80, https://doi.org/10.1016/j.jenvman.2019.04.077.